GEOPHYSICAL RESEARCH LETTERS, VOL. 25, NO.14, PAGES 2625-2628, JULY 15, 1998

Plasma and magnetic field structure of a slow shock: Wind observations in interplanetary space

Y. C. Whang

Catholic University of America, Washington, D.C. 20064

D. Larson and R. P. Lin

Space Sciences Laboratory, University of California, Berkeley, CA 94720

R. P. Lepping and A. Szabo

NASA Goddard Space Flight Center, Greenbelt, MD 20771

Abstract. This paper reports on the observation of an interplanetary slow shock on May 23, 1995 using 3-s plasma and magnetic field data from the Wind spacecraft. Since the time to traverse the shock (~15 s) is much greater than the 3-s temporal resolution of the data, this observation can reveal the plasma and magnetic field structure through the interior of the shock. The 3-s data also provide accurate preshock and postshock conditions immediately outside the shock layer. The flow speeds in the shock frame of reference $U_n < a \cos \Theta$ on both sides of the shock, $U_{n1} > C_{S1}$, and $U_{n2} < C_{S2}$. Here a and C_S are, respectively, the Alfven speed and the slow speed, Θ is the acute angle between the magnetic field vector and the shock normal, and the subscripts 1 and 2 denote the preshock and the postshock conditions. $\Theta_1 \sim 47°$ and $\Theta_2 \sim 39°$. The jump conditions B_2/B_1, N_2/N_1, and $(T_i + T_e)_2 / (T_i + T_e)_1$ of the observational result are in good agreement with the Rankine-Hugoniot solution. The thickness of the shock is of the order of 36 times of the preshock ion inertial length.

Introduction

In the past thirty years, a small number of slow shocks have been observed in interplanetary space [*Chao* and *Olbert*, 1970; *Burlaga* and *Chao*, 1971; *Richter* et al., 1981; and *Whang* et al., 1996]; and a few dozen slow shocks have been observed in the magnetotail [*Feldman* et al., 1985, 1987; *Smith* et al., 1984; *Seon* et al., 1995; and *Saito* et al., 1995].

Recently, it has been reported that many slow shocks are followed by adjoining rotational discontinuity layers on the postshock side [*Whang* et al, 1997, 1998]. Across the rotational layer the magnetic field rotates by a large angle about the normal direction, while its magnitude almost remains constant. The two successive discontinuities of a slow shock layer and a rotational layer are very close to each other. Such a compound structure looks like a new kind of MHD discontinuity; it may be called a double discontinuity. However, not all slow shocks are accompanied by a rotational discontinuity; some slow shocks are stand-alone slow shocks not accompanied by a rotational discontinuity. About a dozen double discontinuities have been identified in interplanetary space and in the magnetotail using high-resolution magnetic field data obtained from Wind, Geotail, Imp-8 and ISEE-3 spacecraft. From Wind data we notice that, in interplanetary space the observations of double discontinuities are no less frequent than the observations of stand-alone slow shocks.

The temporal resolutions vary over a wide range for observational data obtained from various instruments. The high-resolution magnetic field data are usually available at rates better than several vectors per second. These data have sufficient time-resolution to describe the detailed magnetic field structure in the interior of a slow shock or a double discontinuity.

The temporal resolution of the plasma data used in studying slow shocks is poorer than that of the magnetic field data. The best resolution of plasma data for previous study of interplanetary slow shocks reported in literature was 40.5 s for the observations made by Helios 1 at 0.31 AU [*Richter* et al., 1981]. These data do not have sufficient time-resolution to reveal the detailed plasma structure inside the shock. Because of insufficient time-resolution, it is also difficult to evaluate the accuracy of the plasma conditions immediately outside the shock layer.

This paper reports on the observation of a stand-alone slow shock in interplanetary space identified from plasma and magnetic field instruments on the Wind spacecraft on May 23, 1995. High-resolution (0.092-s) magnetic field data have been used to show that this shock is not accompanied by a rotational discontinuity on the postshock side. This is a relatively thick stand-alone slow shock in interplanetary space, the spacecraft traversed the shock layer in ~15 s. The plasma data obtained from Wind 3D Plasma and Energetic Particles Instrument have a time resolution of 3 s which is much better than the time-scale of shock thickness. We can use 3-s plasma and magnetic field data to examine the variation of plasma and magnetic field across the shock. This observation can simultaneously reveal the plasma and magnetic field structure through the interior of the slow shock.

If accurate preshock and postshock conditions of plasma and magnetic field are available from observational data immediately outside the shock layer, methods to study the MHD shock have been very well developed by many authors [*Colburn and Sonett*, 1966; *Lepping and Argentiero*, 1971; *Abraham-Shrauner* and *Yun*, 1976; *Acuña and Lepping*, 1984; *Viñas and Scudder*, 1986; *Smith and Burton*, 1988; *Szabo*, 1994; and *Whang* et al., 1996]. Flow parameters on either side of a shock can be represented by some average conditions of a few data points. Previous studies of interplanetary slow shocks typically use two subsets of data on both sides of a shock at a separation of several minutes apart. This separation is much greater than the shock thickness. Furthermore, over a time interval of several minutes, the flow conditions vary substantially on both sides of the shock. It becomes difficult to justify that these average conditions can represent the

Paper number 98GL02043.
0094-8534/98/98GL-02043$05.00

preshock and postshock conditions. Making use of 3-s plasma and magnetic field data in this study, we can obtain accurate preshock and postshock conditions immediately outside the shock layer for Rankine-Hugoniot analysis of the shock.

Magnetic field observation

Figure 1 shows 60 s of the 3-s magnetic field data from Wind on May 23, 1995. B is the magnitude of the magnetic field and the directional angles are

$$\phi = \arctan\left(B_y / B_x\right) \qquad \theta = \arctan\left(B_z / \sqrt{B_x^2 + B_y^2}\right).$$

Here B_x, B_y, B_z are three components of the magnetic field in geocentric solar ecliptic (GSE) coordinate system. The thickness of the observed shock layer has a time-scale of ~15 seconds. Observation of the shock began at t_1 ~1720:38 and ended at t_2 ~1720:53. The data describe the magnetic field structure through the interior of a forward slow shock. We use two subsets of the observational data over a 15-second period before t_1 and after t_2 to represent the conditions on the preshock side and the postshock side. The averages of the 3-s magnetic field data are 15.4 nT on the preshock side and 13.4 nT on the post shock side. The rms deviations of the 3-s magnetic field data over a 15-s period before t_1 and after t_2 are 0.91 nT and 0.36 nT, respectively (Table 1). The magnetic field is quite steady on both sides of the shock.

Let $\mathbf{n} = n_x\,\mathbf{i} + n_y\,\mathbf{j} + n_z\,\mathbf{k}$ be the unit normal vector of the shock layer pointing in the direction of the mass flow. The divergence free condition of magnetic field requires that along the **n** direction the variation in magnetic field component should be a minimum. An analysis of the 3-s magnetic field data determines the three directional angles of the unit normal vector $\cos^{-1} n_x = 74°$, $\cos^{-1} n_y = 41°$, and $\cos^{-1} n_z = 53°$. The normal component of the magnetic field B_n is –10.4 nT and the rms deviation of B_n is 0.14 nT. As the minimum variance analysis is used here, we check the out-of-coplanarity component of the magnetic field B_s. Although B_s is not zero inside the shock layer, we choose the n,t,s coordinate system in such a way that the average of B_s is zero inside the shock layer; their rms deviation is 0.41 nT. The shock angle Θ is the acute angle between the shock normal and the magnetic field; Θ_1 ~ 47° in the preshock side and Θ_2 ~ 39° in the postshock side.

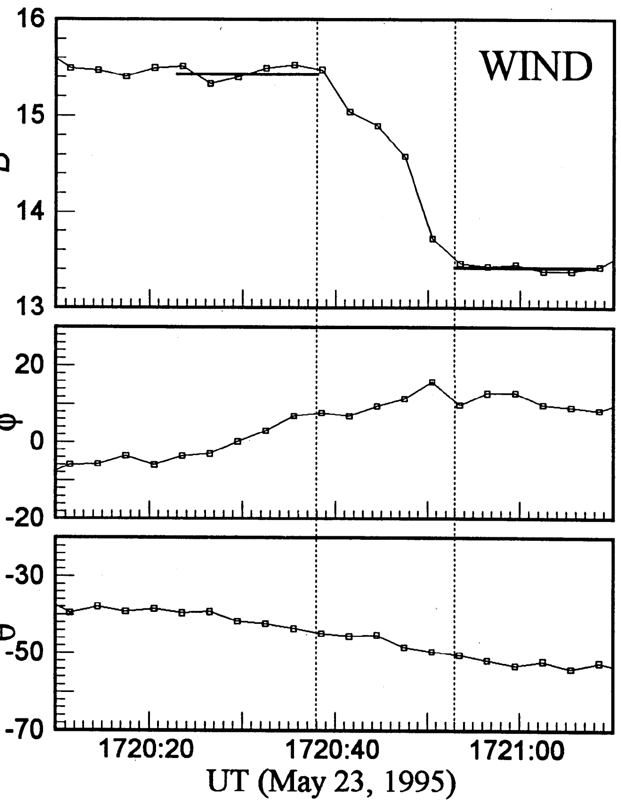

Figure 1. A slow shock observed from 3-s magnetic field data from Wind. The thickness of the shock layer has a time-scale of ~15 seconds.

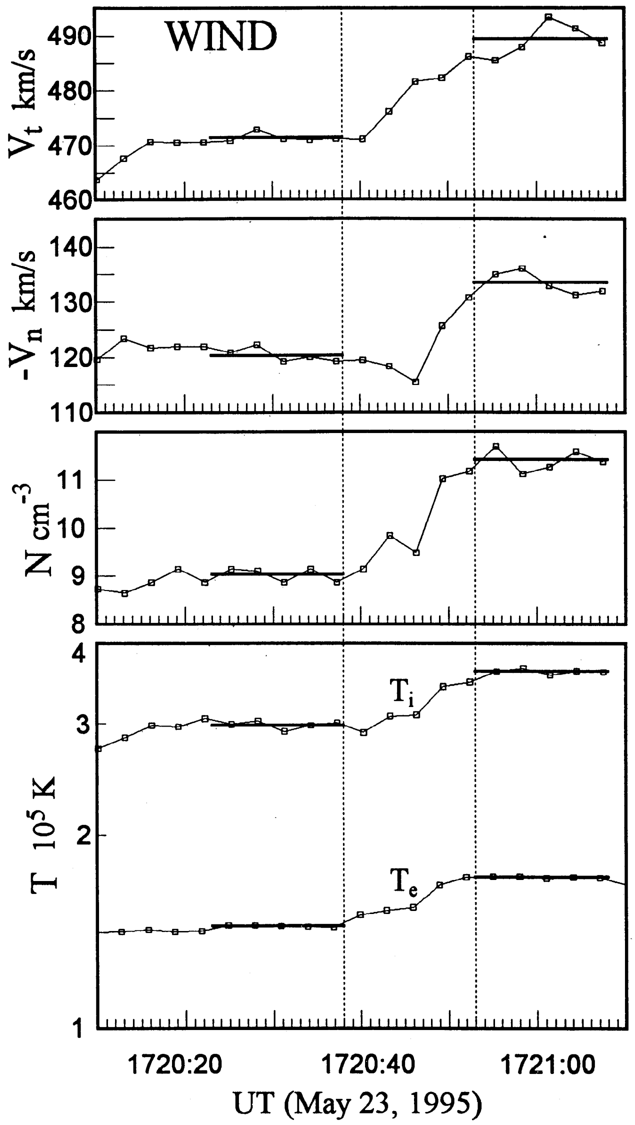

Figure 2. Simultaneous 3-s plasma data are available to show the plasma structure of the observed slow shock.

Plasma observation

Figure 2 shows 60 s of 3-s plasma data: the tangential component of the bulk flow velocity V_t, the normal component of the bulk flow velocity V_n, the number density N, the proton temperature T_i, and the electron temperature T_e.

Table 1 shows the averages and the rms deviations of the 3-s data over 15-s periods before t_1 and after t_2. These averages are used to represent the plasma conditions immediately outside the observed slow shock (V_{1n}, V_{2n}, N_1, N_2, T_{i1}, T_{i2}, T_{e1}, and T_{e2}). The calculated rms deviations indicate that the plasma flow is reasonably steady on both sides of the shock. Across the shock structure the number density increases by a factor of 1.3, the proton temperature increases by a factor of 1.21, the electron temperature increases by a factor of 1.19, while the magnitude of magnetic field decreases by a factor of 0.87. The plasma β changes from $\beta_1 = 0.58$ to $\beta_2 = 1.2$. The increase of entropy per proton across the shock layer can be calculated from [*Whang*, et al. 1989]

$$[s_i] = \mathrm{k} \ln\left\{\left(\frac{T_{i2}}{T_{i1}}\right)^{1.5} \frac{N_1}{N_2}\right\}$$

where k is the Boltzmann constant. The entropy increase across this slow shock is 7×10^{-18} erg/K. The changes in the plasma and magnetic field properties across the shock layer are consistent with those expected for a forward slow shock.

In the inertial frame of reference the shock propagation speed (normal to the shock surface) can be calculated from

$$S = \pm\frac{N_1V_{1n} - N_2V_{2n}}{N_2 - N_1}$$

and the bulk velocity of the solar wind in the shock frame of reference is

$$\mathbf{U} = \mathbf{V} \pm S\mathbf{n}$$

Here the upper sign is for forward shocks, and the lower sign is for reverse shocks. $S = 182$ km/s for the observe slow shock. As shown in Table 2, from the observational data we have the relative flow speeds $U_n < a \cos \Theta$ on both sides of the shock, $U_{n1} > C_{S1}$ on the preshock side, and $U_{n2} < C_{S2}$ on the postshock side. Here a is the Alfven speed and C_S is the slow speed. Calculations use the ratio of the specific heats $\gamma = 5/3$.

Since we have the shock speed in the shock normal direction, as shown in Table 3 we can calculate that the thickness of the observed slow shock is of the order of 36 times of the preshock ion inertial length.

Summary and discussions

The exact solutions of slow shocks have been extensively studied in the past forty years. The jump conditions can be calculated as functions of three dimensionless preshock conditions: the shock Alfven number $A_1 = U_{1n}/a_1 \cos \Theta_1$, the preshock β_1, and the shock angle Θ_1 [*Whang*, 1987, 1988]. The shock Alfven number A_1 is less than 1 for slow shocks. Table 2 also shows the Rankine-Hugoniot solution with $A_1 = 0.81$, $\beta_1 = 0.58$, and $\Theta_1 =$ 47° for the observed slow shock. The calculated B_2/B_1, N_2/N_1, and $(T_i + T_e)_2 / (T_i + T_e)_1$ are in reasonably good agreement with the observational result.

Table 1. Plasma and Magnetic Field Conditions.

Paramters	Preshock Average	Preshock rms	Postshock Average	Postshock rms
B, nT	15.4	0.91	13.4	0.36
V_n, km/s	−120	1.1	−133	1.8
V_t, km/s	471	0.8	489	2.7
N, cm^{-3}	9.0	0.13	11.4	0.21
T_i, K	2.99×10^5	380	3.62×10^5	290
T_e, K	1.44×10^5	410	1.72×10^5	400

Table 2. Observed and Calculated Conditions of the Slow Shock.

Shock Parameters	
Preshock conditions (observation)	
β_1	0.58
Θ_1	47°
U_{1n} (km/s)	62
$U_{1n}/a_1 \cos \Theta_1$	0.81
U_{1n}/C_{S1}	1.33
Postshock conditions (observation)	
β_2	1.2
Θ_2	39°
U_{2n} (km/s)	49
B_2/B_1	0.87
N_2/N_1	1.3
$(T_i + T_e)_2 / (T_i + T_e)_1$	1.2
$U_{2n}/a_2 \cos \Theta_2$	0.73
U_{2n}/C_{S2}	0.93
Rankine-Hugoniot solutions	
β_2	1.6
Θ_2	34°
U_{2n} (km/s)	44
B_2/B_1	0.82
N_2/N_1	1.4
$(T_i + T_e)_2 / (T_i + T_e)_1$	1.3
$U_{2n}/a_2 \cos \Theta_2$	0.68
U_{2n}/C_{S2}	0.79

The time-scale for the thickness of this shock (~15 s) is unusually long in comparison with other interplanetary slow shocks we have observed from Wind data [*Whang* et al, 1996, 1998]. Because of this long time-scale, it becomes possible to see simultaneously the plasma and the magnetic field structure of the shock layer using 3-s data from Wind. The long time-scale of this observation can be attributed to the geometrical reason that the shock normal makes a large angle of 74° with the solar wind direction. This large angle increases by a factor of 3 the duration in which the spacecraft stayed in the interior of the shock layer.

The second reason for the long time-scale of this observation is related to the strength of the shock. The shock thickness decreases for stronger shock [*Hayes*, 1960]. The observed shock is a relatively weak shock with a slow Mach number of 1.33.

The dynamical process of a shock layer involves a diffusion process and a convection process. Theoretical aspects for the merging of slow-mode MHD waves to form slow shocks have been studied by *Barnes* [1979] using a kinetic theory approach and by *Whang* [1991, 1996, 1997] using a continuum MHD approach. These studies explain the processes responsible for Landau damping and diffusive attenuation of slow-mode waves and the steepening of the compression wave front to form slow shocks. The diffusion effect tends to increase the thickness of a shock layer, whereas the dynamical convection effect tends to decrease the shock thickness. A shock maintains a particular thickness as the two effects reach a dynamical equilibrium state [*Lighthill*, 1956]. Our interpretation for the formation of a slow shock accompanied by a rotational layer is that the rotational discontinuity approaches the slow shock from the postshock side. Somehow the rotational discontinuity can not penetrate through the shock layer and the two layers merge into a stable compound structure. The dynamic interaction between the two layers would compress the shock layer to reduce its thickness. The observed shock of May 23, 1995 is a stand-alone slow shock; no dynamical interactions of the shock with rotational discontinuity are

Table 3. The Thickness of the Observed Slow Shock.

	April 6, 1995
Crossing time Δt , s	15
Shock speed S, km s^{-1}	182
Shock thickness $S\Delta t$, km	2734
Number density N_1, cm^{-3}	9
Ion inertial length λ_1, km	77
$S\Delta t / \lambda_1$	36

visible in the high-resolution data. Hence, the time-scale of this stand-alone slow shock is longer than the time-scales of all double discontinuities that have been observed in interplanetary space.

This paper presents the observations of MHD parameters across a slow shock. A referee suggested the importance of studying the kinetic description of the shock crossing. We agree with the suggestion. 3D Plasma data can be used to study the variations of major characteristics of the velocity distributions across the shock layer.

Acknowledgments. The work at the Catholic University of America was supported by NASA grant NAG-52814. The WIND 3D Plasma and Energetic Particle experiment data analysis is supported at Berkeley by NASA grant NAG-52815.

References

Abraham-Shrauner, B., and S. H. Yun, Interplanetary shocks seen by Ames plasma probe on Pioneer 6 and 7, *J. Geophys. Res.*, *81*, 2097, 1976.

Acuña, M. H., and R. P. Lepping, Modification to shock fitting program, *J. Geophys. Res.*, *89*, 11,004, 1984.

Barnes, A., Hydromagnetic waves and turbulence in the solar wind, in *Solar System Plasma Phys., vol. 1*, p. 276-319, edited by E. N. Parker, C. F. Kennel, and L. J. Lanzerotti, North-Holland, New York, 1979.

Burlaga, L. F., and J. K. Chao, Reverse and forward slow shocks in the solar wind, *J. Geophys. Res.*, *76*, 7516, 1971.

Chao, J. K., and S. Olbert, Observation of slow shocks in interplanetary space, *J. Geophys. Res.*, *75*, 6394, 1970.

Colburn D. S. and C. P. Sonett, Shock in the solar wind, *Space Sci. Rev.*, *5*, 439, 1966.

Feldman, W. C., D. N. Baker, S. J. Bame, J. Birn, J. T. Gosling, E. W. Hones, Jr., and S. J. Schwartz, Slow mode shocks: A semipermanent feature of the distant geomagnetic tail, *J. Geophys. Res.*, *90*, 233, 1985.

Feldman, W. C., R. L. Tokar, J. Birn, E. W. Hones, Jr., S. J. Bame, and C. T. Russell, Structure of a slow mode shock observed in plasma sheet boundary layer, *J. Geophys. Res.*, *92*, 83, 1987.

Hayes, W. D., Gasdynamic Discontinuities, Princeton University press, 35-50, 1960.

Lepping, R. P., and P. D. Argentiero, Single spacecraft method of estimating shock normal, *J. Geophys. Res.*, *76*, 4349, 1971.

Lighthill, M. J., Viscosity effects in sound waves of finite amplitude, in *Surveys in Mechanics*, Ed. by G. K. Batchelor and R. M. Davies, (Cambridge University Press), 264, 1956.

Richter, A. K., H. Rosenbauer, F. M. Neubauer, and N. G. Ptitsyna, Solar wind observations associated with a slow-forward shock wave at 0.31 AU, *J. Geophys. Res.*, *90*, 7581, 1985.

Saito, Y., T. Mukai, T. Terasawa, A. Nishida, S. Machida, M. Hirahara, K. Maezzawa, and T. Yamamoto, Slow-mode shocks in the magnetotail, *J. Geophys. Res.*, *100*, 23,567, 1995.

Seon, J., L. A. Frank, W. R. Paterson, J. D. Scudder, F. V. Coroniti, S. Kokubun, and T. Yamamoto, Observations of a slow-mode shock at the lobe-plasma sheet boundary in Earth's distance magnetotail, *Geophys. Res. Lett.*, 22, 2981, 1995.

Smith, E. J., J. A. Slavin, B. T. Tsurutani, W. C. Feldman, and S. J. Bame, Slow mode shocks in the earth's magnetotail: ISEE-3, *Geophys. Res. Lett.*, *11*, 1054, 1984.

Smith, E. J., and M. E. Burton, Shock analysis: three useful new relations, *J. Geophys. Res.*, *93*, 2730, 1988.

Szabo, A., An improved solution to the "Rankine-Hugoniot" problem, *J. Geophys. Res.*, *99*, 14,737, 1994.

Viñas, A. F., and J. D. Scudder, Fast and optimal solution to the Rankine-Hugoniot problem, *J. Geophys. Res.*, *91*, 39, 1986.

Whang, Y. C., Slow shocks and their transition to fast shocks in the inner solar wind, *J. Geophys. Res.*, *92*, 4349-4356, 1987.

Whang, Y. C., Evolution of interplanetary slow shocks, *J. Geophys. Res.*, *93*, 251-255, 1988.

Whang, Y. C., Parametric study of the formation of magnetohydrodynamic shocks, II. slow shocks, *Astrophys. J.*, *377*, 255-262, 1991.

Whang, Y. C., Merging of slow-mode compressive waves in low-β plasma, *J. Geophys. Res.*, *101*, 2529, 1996.

Whang, Y. C., Attenuation of magnetohydrodynamic waves, *Astrophys. J.*, *485*, 389, 1997.

Whang, Y. C., K. W. Behannon, L. F. Burlaga, and S. Zhang, Thermodynamic properties of the heliospheric plasma, *J. Geophys. Res.*, *94*, 2345, 1989.

Whang, Y. C., J. Zhou, R. P. Lepping, and K. W. Ogilvie, Interplanetary slow shock observed from Wind, *Geophys. Res. Lett.*, *23*, 1239, 1996.

Whang, Y. C., D. Fairfield, E. J. Smith, R. P. Lepping, S. Kokubun, and Y. Saito, Observations of Double Discontinuities in the Magnetotail, *Geophysical Research Letters*, *24*, 3153, 1997.

Whang, Y. C., J. Zhou, R. P. Lepping, A. Szabo, D. Fairfield, S. Kokubun, K. W. Ogilvie, and R. Fitzenreiter, Double Discontinuity: A Compound Structure of Slow Shock and Rotational Discontinuity, *J. Geophys. Res.*, *103*, 6513, 1998.

D. Larson and R. P. Lin, Space Sciences Laboratory, University of California, Berkeley, CA 94720

R. P. Lepping and A. Szabo, NASA Goddard Space Flight Center, Greenbelt, MD 20771

Y. C. Whang, Dept. of Mechanical Engineering, Catholic University of America, Washington, D.C. 20064, (e-mail: whang@cua.edu)

(Received March 12, 1998; revised June 2, 1998; accepted June 5, 1998.)